FERMILAB-CONF-11-481

CMS: Present Status, Limitations, and Upgrade Plans

H. W. K. Cheung
for the CMS collaboration

Fermi National Accelerator Laboratory

Operated by Fermi Research Alliance, LLC under Contract No. De-AC02-07CH11359 with the United States Department of Energy

Abstract

An overview of the CMS upgrade plans will be presented. A brief status of the CMS detector will be given, covering some of the issues we have so far experienced. This will be followed by an overview of the various CMS upgrades planned, covering the main motivations for them, and the various R&D efforts for the possibilities under study.

Keywords:

1. Introduction

The CMS detector has been working extremely well since the start of data-taking at the LHC as is evidenced by the numerous excellent results published by CMS and presented at this workshop and recent conferences. Less well documented are the various issues that have been encountered with the detector. In the spirit of this workshop I will cover some of these issues with particular emphasis on problems that motivate some of the upgrades to the CMS detector for this decade of data-taking.

As part of the presentation of the CERN "10 Year Technical Plan" for the operation of the LHC collider [1], preliminary expectations for the luminosity of the LHC was given for this decade. Table 1 shows the predictions for some of the parameters given for the LHC and the upgraded High Luminosity LHC (HL-LHC) through 2020. At the end of the Phase 1 period in 2020, the LHC is expected to have delivered over 300 fb^{-1}. About 65% of this integrated luminosity is expected in the final two years, running at a peak luminosity above 10^{34} $cm^{-2}s^{-1}$, the design for the LHC. The highest luminosity expected for this Phase 1 period of the HL-LHC is about 2.2×10^{34} $cm^{-2}s^{-1}$. Although the schedule and predictions are now somewhat out-of-date, it still gives a reasonable indication of the expected luminosity profile.

Above the 10^{34} $cm^{-2}s^{-1}$ design luminosity of the LHC, the performance of the CMS detector and trigger is expected to degrade; this is detailed in the Technical Proposal for the upgrade of the CMS detector [2]. These expected degradations add further motivation for the proposed upgrades to the CMS detector.

2. Current Status

The current status of the CMS detector is covered by the presentation of E. Focardi [3], so only a few selected features will be highlighted in this section.

Year	TeV	OEF	β*	Nb	Ib	Itot	MJ	Peak luminosity	Pile up	pb-1/day	Physics Days	Integrated (fb-1/year)	Total Int (fb-1)
2010	3.50	0.20	2.00	796	8.0E+10	6.4E+13	36.0	1.886E+32	1.2643	3.3	20.0	0.1	0.07
2011	3.50	0.25	2.00	796	8.0E+10	6.4E+13	36.0	1.886E+32	1.2643	4.1	240.0	0.98	1.04
2012												0.0	1.0
2013	6.50	0.20	0.55	796	1.15E+11	9.2E+13	96.1	2.632E+33	17.6429	45.5	180.0	8.2	9.2
2014	7.00	0.20	0.55	1404	1.15E+11	1.6E+14	182.5	5.000E+33	19.0000	86.4	240.0	20.7	30.0
2015	7.00	0.20	0.55	2808	1.15E+11	3.2E+14	365.0	1.000E+34	19.0000	172.8	210.0	36.3	66.3
2016											0.0	0.0	66.3
2017	7.00	0.25	0.55	2808	1.15E+11	3.2E+14	365.0	1.000E+34	19.0000	216.0	240.0	51.8	118.1
2018	7.00	0.28	0.55	2808	1.50E+11	4.2E+14	476.1	1.701E+34	32.3251	411.6	240.0	98.8	216.9
2019	7.00	0.30	0.55	2808	1.70E+11	4.8E+14	539.6	2.185E+34	41.5198	566.4	210.0	118.9	335.8
2020											0.0	0.0	335.8
2021	7.00	0.20	0.30	2808	1.70E+11	4.8E+14	539.6	4.006E+34	76.1197	692.3	150.0	103.8	439.7
2022	7.00	0.27	0.25	2808	1.80E+11	5.1E+14	571.3	5.390E+34	102.4060	1257.3	220.0	276.6	716.3
2023	7.00	0.27	0.25	2808	1.80E+11	5.1E+14	571.3	5.390E+34	102.4060	1257.3	220.0	276.6	992.9
2024	7.00	0.29	0.25	2808	1.80E+11	5.1E+14	571.3	5.390E+34	102.4060	1350.5	220.0	297.1	1290.0
2025	7.00	0.29	0.25	2808	1.80E+11	5.1E+14	571.3	5.390E+34	102.4060	1350.5	220.0	297.1	1587.1
2026	7.00	0.29	0.25	2808	1.80E+11	5.1E+14	571.3	5.390E+34	102.4060	1350.5	220.0	297.1	1884.2
2027	7.00	0.29	0.25	2808	1.80E+11	5.1E+14	571.3	5.390E+34	102.4060	1350.5	220.0	297.1	2181.3
2028	7.00	0.29	0.25	2808	1.80E+11	5.1E+14	571.3	5.390E+34	102.4060	1350.5	220.0	297.1	2478.4
2029	7.00	0.29	0.25	2808	1.80E+11	5.1E+14	571.3	5.390E+34	102.4060	1350.5	220.0	297.1	2775.5
2030	7.00	0.29	0.25	2808	1.80E+11	5.1E+14	571.3	5.390E+34	102.4060	1350.5	220.0	297.1	3072.6

Fig. 1. The expected luminosity for each year of LHC operations between 2010 and 2020 [1, 2]. Included in the table are the energy per beam in TeV; the peak luminosity in $cm^{-2}s^{-1}$; the pile up, which is the average number of interactions per crossing at the peak luminosity; and the integrated luminosity/year in fb^{-1}. The design crossing time of 25 ns is assumed. The last column shows the integrated luminosity from the beginning of the LHC program in 2010 in fb^{-1}.

Although the performance of the CMS detector has been excellent, there have of course been issues that were encountered. Some of the problems are ones that are expected in any new complex detector, for example 4.6% of the pixel detector channels are not currently working, these are due to a variety of random electronic issues some of which can be recovered given sufficient access time to the detector [4]. However there hare been some issues that were less expected. An example of an issue that initially caused some problem at low luminosity was beam gas interactions in the straight section of the LHC leading to higher than expected readout rates for the pixel detector. Particles traveling almost parallel to the beam axis at the radius of a pixel barrel layer could cross a pixel sensor and cause a large number of pixels hits in a single readout channel resulting in a timeout and lost data. This was resolved by a modif ed f rmware to dump long events and holdoff triggers. The rate of these scales with the beam intensity, and at the current high luminosities it is now low compared to the collision rate.

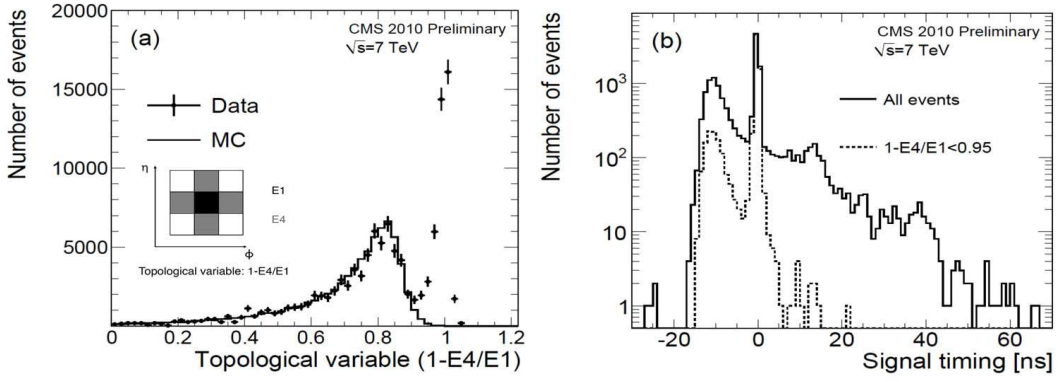

Fig. 2. Characteristics of anomalous ECAL signals (a) topological, (b) timing.

Another example of an anomalous signal is from the barrel electromagnetic calorimeter, which had the appearance of large energy deposits in a single crystal that can affect the Level 1 trigger. The origin of these turned out to be heavily ionizing particles interacting in the avalanche photodiode (APD) that is used for the photodetector, and can occur at a rate of 1 in 1000 minimum bias events. At the cluster level the anomalous signals appear as energy in a single crystal, while in electromagnetic showers the energy is typically shared between neighbouring crystals. The anomalous signals typically also have different timing. These topological and timing characteristics are shown in Fig. 2 and are used to f lter out these anomalous signals reducing them to a manageable rate in the Level 1 trigger.

In the following sections, some of the other detector issues that were encountered, or are expected to be an issue for luminosities above the LHC design are discussed in relation to proposed upgrades. A more complete and detailed description of the CMS upgrades is given in the CMS upgrade proposal [2].

3. Upgrade to Muon Systems

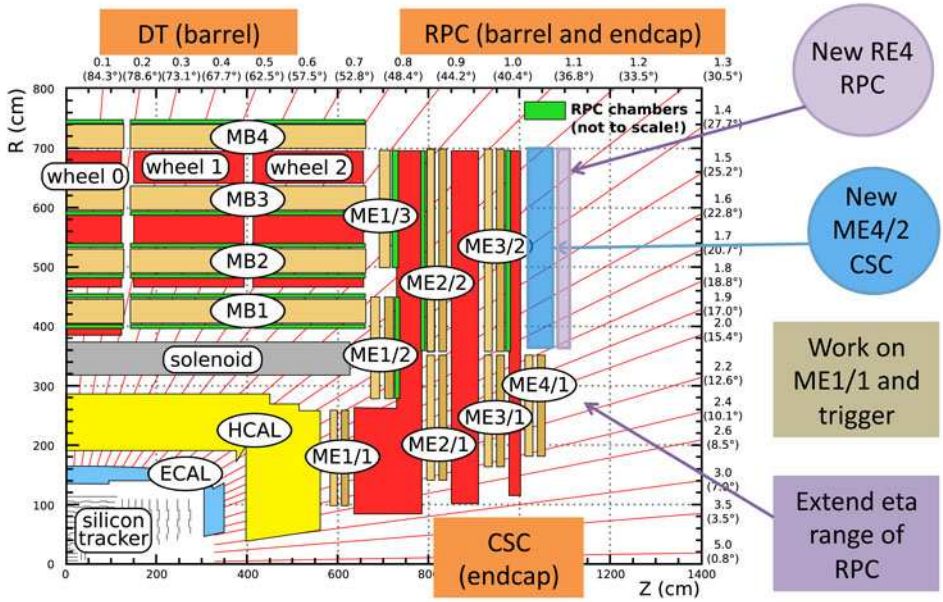

Fig. 3. Schematic view of the CMS muon detector.

Figure 3 shows a schematic view detailing the CMS muon detector system and summarizing the proposed upgrades to the muon system. Drift tube (DT) chambers are employed in the barrel region while cathode strip chambers (CSC) are used in the two endcap regions. These are augmented in both barrel and endcap regions by resistive plate chambers (RPC) providing a fast independent trigger over a large portion of the rapidity range.

At the highest Phase 1 luminosities the CSC trigger track f nder (CSCTF) needs to require 3 segments instead of the current 2 to improve the muon p_T measurement so that the trigger rate is not overwhelmed by mismeasured low p_T muons. This is shown in Figs. 4(a) and (b). The same effect occurs in the RPC system. To improve the efficiency a fourth station of chambers (ME4/2 and RE4) is proposed which will reduce the large and uncertain losses of otherwise requiring perfect muon information from every muon station, *e.g.* see Fig. 4(f).

The ME1/1 CSC muon chamber is the most important station for standalone muon momentum resolution with $|\eta| = 1.6$–2.4 since it is closest to the interaction point and in the region before the magnetic f eld changes direction. However it also receives the highest particle rates of any of the CMS muon chambers as well as

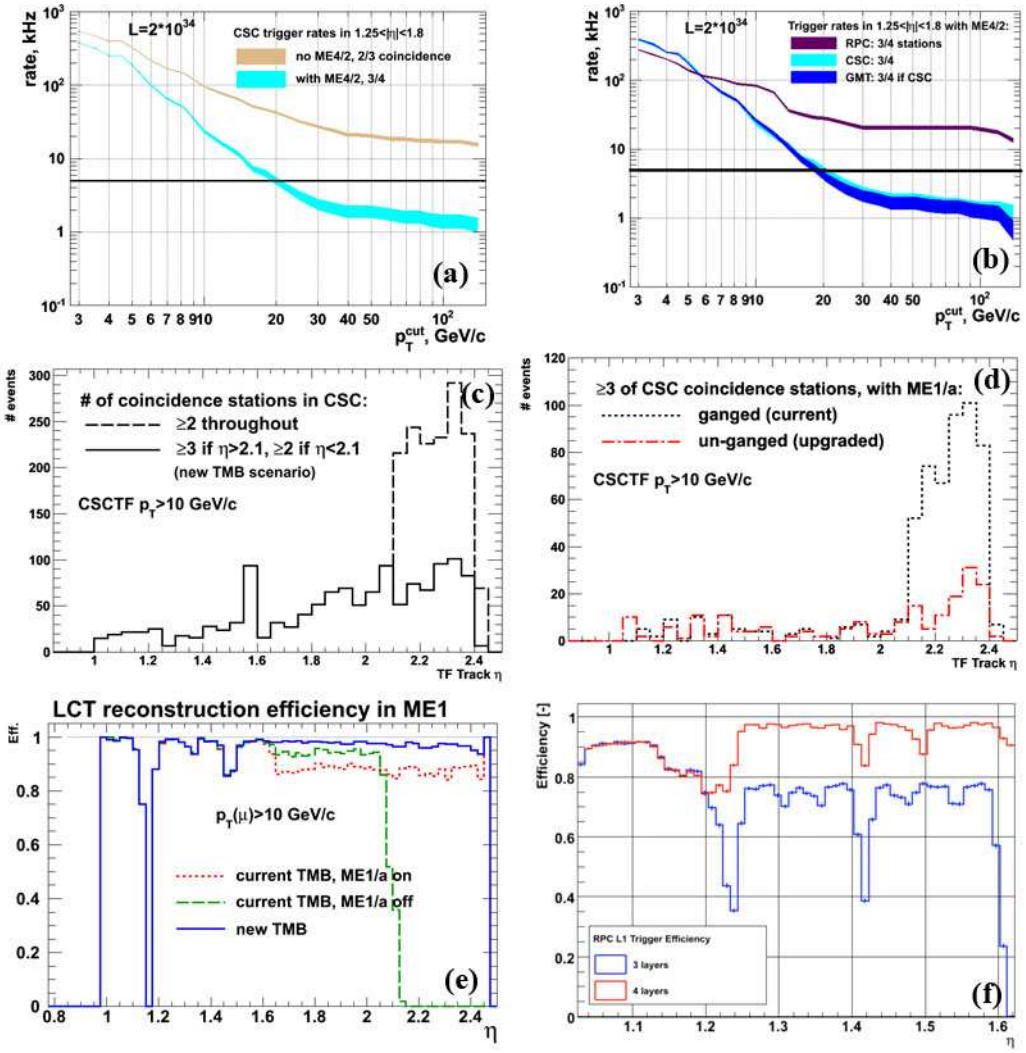

Fig. 4. (a) Simulation predictions for the contribution to the CSC inclusive muon trigger rate from the region $1.25 < |\eta| < 1.8$ as a function of trigger p_T threshold. The curves demonstrate that the CSC trigger performance critically depends on the ME4/2. The target single-muon trigger rate of 5 kHz is indicated by the horizontal line; (b) Trigger rate of the upgraded RPC and CSC systems (including the proposed RE4 and ME4/2 upgrades) as well as the Global Muon Trigger (GMT) rate. The RPC curve shown corresponds to the conf guration optimized for high efficiency and not for rate rejection. (c) Simulation predictions for the pseudorapidity distribution for background events passing the current L1 trigger (dashed line). The enhancement in the region $|\eta| > 2.1$ is due to the strip ganging in ME1/1. For LHC luminosities, the requirement of a three-out-of-four station coincidence and an improved TMB algorithm (solid line) help decrease the rate to an acceptable level. (d) At the highest Phase 1 luminosities the addition of station ME4/2 and requiring a three station match in the entire CSC detector (dotted line) will bring the rate in the lower η range to an acceptable level, however suppressing the large remaining contribution to the trigger rate from $|\eta| > 2.1$ requires unganging the strips in ME1/1 chambers (dash-dotted line); (e) Simulation prediction for the efficiency of f nding a local muon track in station ME1 as a function of muon pseudorapidity for muons with $p_T > 10$ GeV/c. The decrease in efficiency is due to backgrounds from pile-up (note that this calculation includes prompt contributions only, i.e. no beam or neutron backgrounds). Because of the features of the TMB board, the efficiency over the entire range of $|\eta| = 1.6$–2.4 is sensitive to the background rate in the region of $|\eta| = 2.1$–2.4. Upgrade of the TMB board allows recovering robust muon triggering in the entire range of $|\eta| = 1.6$–2.4; (f) Simulated trigger efficiency as a function of the number of layers of RPCs.

high neutron and beam related backgrounds. An important issue was identif ed with the muon trigger that is relevant for the region $|\eta|$ =2.1–2.4 already at design LHC luminosities. The Trigger MotherBoard (TMB) that handles the reconstruction of local muon tracks in the chambers becomes blind to any new muons for several bunch crossings after reconstructing a local track anywhere in the chamber. Since both the high- and low-η regions of the ME1/1 chambers are handled by a single TMB board, the efficiency of muon triggering in the entire region of $|\eta|$ =1.6–2.4 becomes highly sensitive to the rate of backgrounds in the region of $|\eta|$ =2.1–2.4, as can be seen in Fig. 4(e). This can be resolved with an upgrade to the current TMB using a new generation of FPGA chips. While the new TMB algorithm will recover efficiency, one still needs to address the high contribution to the trigger rate coming from the region of $|\eta|$ =2.1–2.4 as shown in Fig. 4(c). To control the rate, the CSCTF will be conf gured to require 3-out-of-4 station coincidence for candidate tracks with $|\eta|$ >2.1, this is sufficient for design LHC luminosities. At the highest Phase 1 luminosities the 3:1 ganging of ME1/1 channels (at intervals of 16 strips) causes a large increase in the muon trigger rate because low-p_T muons are seen as nearly straight (inf nite momentum) if their bending in the magnetic f eld takes them roughly 16 or even 32 strips away. Unganging of the strips in the ME1/1 chamber is proposed which in turn necessitates upgrades of the associated electronics.

Besides the proposed 4th RPC layer (RE4), an extension of the present η coverage to $1.6 < |\eta| < 2.1$ using additional chambers of possibily different technology is being considered for Phase 2 [5, 2].

4. Upgrade to Hadron Calorimeters

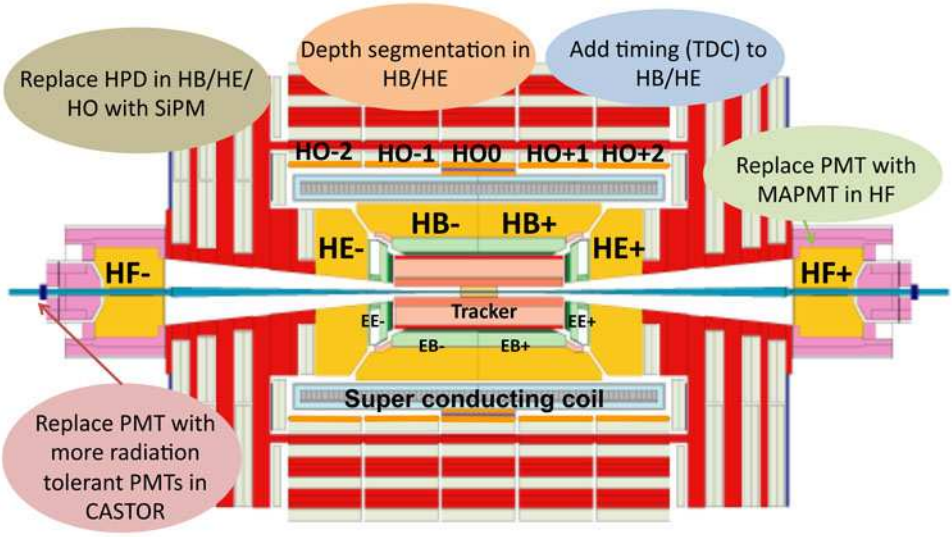

Fig. 5. Schematic view of the CMS Calorimeters.

A schematic view detailing the CMS calorimeter systems is shown in Fig. 5. Anomalous signals were identif ed early in the commissioning of the hadronic calorimeter (HCAL) [6]. The origins of the signals were different between the barrel (HB), endcap (HE), extension (HO), and the forward (HF) sections of the HCAL. Characteristics of the noise in the HB/HE/HO are given in Fig. 6. Ion feedback in the hybrid photodiode (HPD) used in the HB/HE/HO gives rise to noise in mostly a single channel within a HPD. With the HPD operating at ~8 kV in the CMS magnetic f eld, dielectric f ashover from the wall can produce large signals in many channels of a single HPD up to the total number of channels in the HPD (18), this was found to be worse for the HO which is in the region of an intermediate magnetic f eld. Finally there is correlated noise within a readout box (RBX) that houses 4 HPDs that can lead to noise in up to 72 channels, this source is unknown, but is possibly due to external noise coupling to the HV of many channels across the whole RBX. This noise can be f ltered using a combination of topological and timing information [6]. For the HB

and HE the total rate of HPD and RBX noise is 10–20 Hz for $E > 20$ GeV, but the HPD and RBX noise is random and the overlap with physics is very low. The rate for HO is worse and CMS proposes to replace all the HPDs in the HO with silicon photomultipliers (SiPM) in the first long LHC shutdown [7].

In the following long LHC shutdown CMS proposes to also replace the HPDs of the HB and HE with SiPMs. This will eliminate the sources of anomalous signals, and also will improve the front-end signal-to-noise (S/N) by an order of magnitude. This increase in S/N enables other upgrades to the HB and HE that will help them deal with the increased occupancy and timing issues expected for the highest Phase 1 luminosities. The extra space freed up by the use of SiPMs will allow a four-fold increase in longitudinal segmentation to reduce pile-up/high-occupancy performance degradation coming from the first layer of scintillator, to improve clustering and geometric discrimination against non-collision backgrounds and to increase channel redundancy. This leads to expected performance increases for electron isolation and triggering, muon isolation and identification, and energy resolution due to the possibility of compensation for radiation damage front/inner part of the calorimeter. The higher S/N will allow splitting of the signal so time (TDC) measurements per bunch crossing with nanosecond timing resolution down to MIP energies to provide independent rejection for beam halo, cosmic ray, and other non-collision backgrounds.

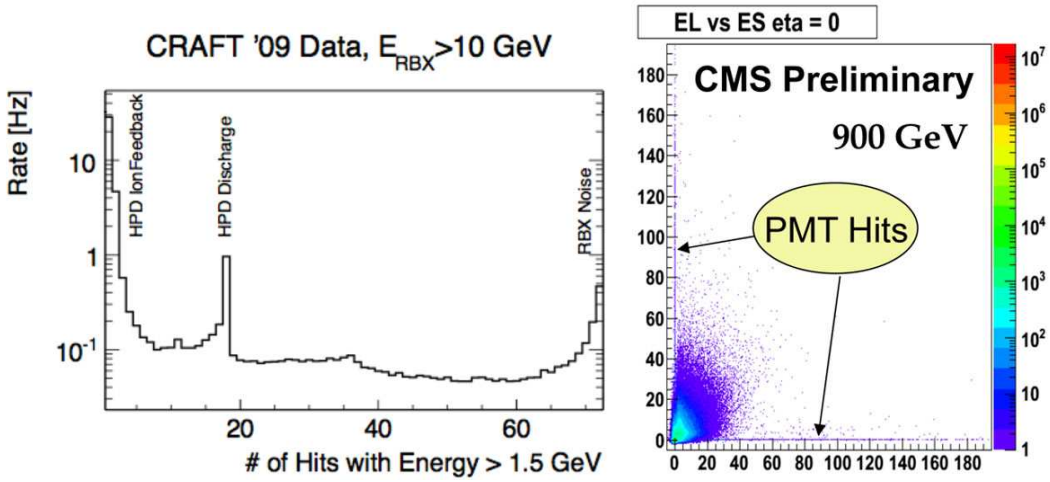

Fig. 6. Characteristics of anomalous HCAL signals. (Left) Number of HCAL (HB/HE/HO) channels within a single RBX with energy greater than 1.5 GeV, for readout boxes with a total energy greater than 10 GeV, for data taken during cosmic running; (Right) Measurements in long fibers versus short fibers in the HF during initial low energy pp collisions.

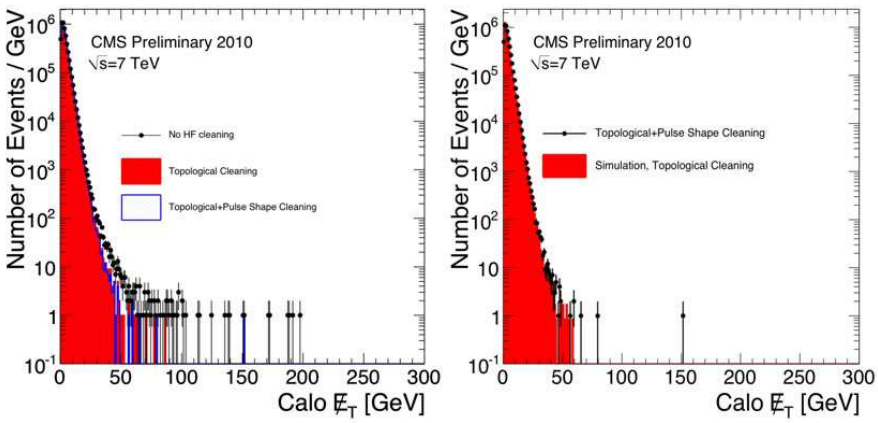

Fig. 7. Missing energy performance after cleaning cuts on HF energy.

Anomalous signals were also seen in the forward hadron calorimeter (HF) where photomultipliers are used as the photodetectors. These were determined to come from particles crossing the PMT glass giving rise to Čerenkov radiation, and appears mostly in one channel at a time in collision data. The dominant sources of particles crossing the PMT glass is muons from decays in flight and hadron punch through at a rate of just less than about ~1 in 1000 minimum bias events. These signals appear as high energy deposits, *e.g.* a 150 GeV muon crossing the PMT glass generates signals equivalent to a 120 GeV pion impacting the HF. These anomalous signals can be recognized topologically. The readout of a HF tower is via a combination of long fibers that extend the full length of the HF and short fibers that start at a depth of 22 cm from the front face of the HF, and these go to separate PMTs. The anomalous signal normally appear only in either the long or the short fiber as can be seen in Fig. 6. In collision data these "PMT events" can give rise to 1 TeV jets. Using a combination of timing information in addition to the afore mentioned topological information these "PMT events" can be tagged offline with an efficiency of about ~80%. The cleaning of these PMT events significantly improves the missing E_T performance as can be seen in Fig. 7. However the ~80% efficiency is still too low for sensitive new physics searches so CMS proposes to replace the HF PMTs with a thin window multi-anode PMT [2]. The much thinner glass reduces the amount of Čerenkov light, while the 4-way segmented anode will allow further rejection of PMT events by using the pattern of light distribution among the anodes, which is different than signals coming from energy deposited in the HF.

5. Pixel Detector Replacement

At the heart of CMS is the silicon pixel detector. It provides three high-precision space point measurements to reconstruct charged particle trajectories, and are sufficient to produce good track information for the High Level Trigger (HLT) and for the efficient seeding of the reconstruction of longer tracks in the full tracker volume. The close proximity of the first detector layer to the interaction point makes the pixel information crucial for the reconstruction of the initial position and direction of the charged tracks. The pixel detector therefore plays a key role in the identification of primary vertices, secondary vertices, and secondary tracks. These elements are essential for the efficient identication of long-lived particles, such as b-quarks, and for the search for new physics at the LHC.

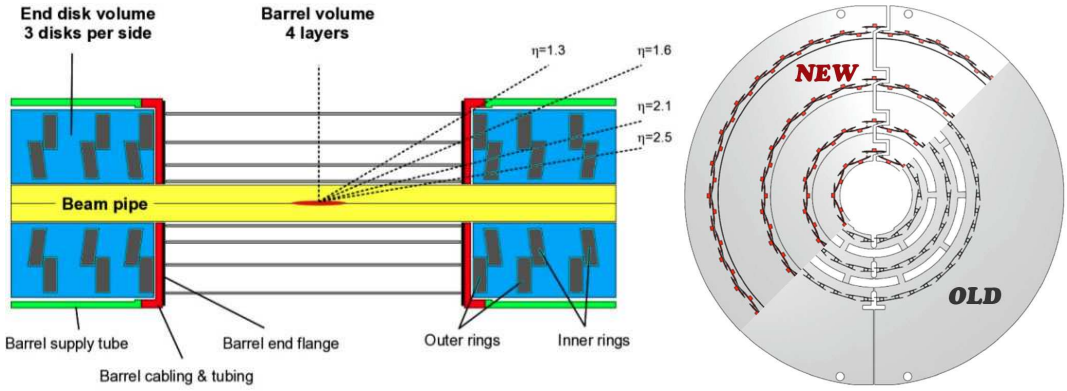

Fig. 8. Schematic view of the upgrade pixel detector. (Left) Side view showing an extra barrel layer at large radius, and an extra forward disk on each end; (Right) Transverse view comparing the barrel layers of the current and upgrade pixel detector.

Above the design luminosity of the LHC, the performance of the pixel detector is expected to degrade significantly. The shortcomings of the current detector are as follows:

- The most severe limitation is the pixel readout chip (ROC), which is just adequate at the LHC design luminosity of 1×10^{34} cm^{-2}s^{-1}. At this luminosity, buffer size and readout speed limitations are estimated to produce a dynamic inefficiency of 4% (>16%) if the bunch spacing time is 25 ns (50 ns). The dynamic inefficiency increases exponentially with increasing luminosity. At 2×10^{34} cm^{-2}s^{-1}

and 25 ns bunch spacing the ROCs in the inner region will suffer an inefficiency of 15%, leading to a major degradation of the overall level of tracking performance.

- The three-hit coverage of the detector is not completely hermetic, leading to 10–15% inefficiencies at $|\eta| < 1.5$ and larger track seeding inefficiencies in the region $1.5 < |\eta| < 2.5$. This limits the efficiency of HLT tracking triggers and slows the full tracking algorithm. The situation will degrade even further at higher luminosities.

- The radiation hardness of the detector is not sufficient for operation up to the end of Phase 1, when the integrated luminosity will be around 350 fb^{-1}. Although the detector was constructed using the most radiation resistant technology known at the time of its fabrication, radiation damage will degrade its performance and necessitate replacement of the inner regions.

- The detector contains signif cant passive material that degrades tracking and calorimetric measurements due to multiple scattering, photon conversions and nuclear interactions.

These shortcomings are addressed by a proposed replacement of the current pixel detector that can maintain a high efficiency at a luminosity of 2×10^{34} cm^{-2}s^{-1}, with less material, and will provide 4 hits over pseudorapidities up to 2.5. The proposed upgrade pixel detector will include an extra layer with a redesigned ROC. A higher bandwidth readout and DC-DC converters will be implemented so that the existing cables and f bers can be reused, even though the number of pixel channels will increase by 70%. Material in the pixel system will be reduced by the use of two-phase CO_2 cooling instead of liquid C_6F_{14}, and by using light-weight mechanical supports and moving electronic boards and connections out of the tracking volume. A smaller diameter beampipe will be installed so that the innermost pixel layer can be located closer to the interaction point.

At the highest Phase 1 luminosities the addition of extra layers will dramatically improve the efficiency and resolution of pixel-only tracks. Pixel tracks are a crucial part of the High Level Trigger (HLT) and they are also used to seed the full tracking, leading to an increase of the efficiency and a decrease of the fake rate for full tracks. The high occupancies lead to unmanageably high combinatorics for tracking seeds made of pairs of pixel hits that are currently used in the tracking. To reduce the resulting high fake track rates, and high CPU and memory usage, only seeds made of 3 pixel hits are used. With the current pixel detector this 3-hit-out-of-3-layers requirement leads to signif cant loss of efficiency especially including the data loss due to the ROC.

The expected improvements in tracking reconstruction efficiency and reduction in track fake rates have been studied with a full Geant4 [8] simulation. The results for the track reconstruction efficiency and track fake rates for $pp \rightarrow t\bar{t}X$ interactions at $\sqrt{s} = 14$ TeV and a luminosity of 2×10^{34} cm^{-2}s^{-1} assuming a crossing time of 25 ns are given in Fig. 9. It can be seen that the tracking efficiency is signif cantly improved while the track fake rates are also reduced especially at low p_T.

The track impact parameter resolution is improved for the upgrade pixel detector [9, 2], and combined with the the efficiency enhancement this leads to much improved primary and secondary vertexing. These improvements can be seen in the performance of the combined secondary vertex b-tagging algorithm, that uses both secondary vertex and track impact parameter information [10]. A comparison of the expected performance as determined in a full Geant4 simulation for the current and upgrade pixel detectors are given in Fig. 10. At a luminosity of 2×10^{34} cm^{-2}s^{-1} and assuming a crossing time of 25 ns, it can be seen that for example, at a f xed b-tagging efficiency of 60% for b-jets, the mistag rate of light quark and gluon jets as b-jets drops by a factor of about seven from about 5×10^{-2} for the current pixel detector to about 7×10^{-3} for the upgrade pixel detector. Conversely for a f xed light quark mistag rate of 1×10^{-2}, the expected b-tagging efficiency for b-jets can be improved by an absolute 18%, from 46% to 64% (a relative 40% improvement) using the upgrade pixel detector. In fact the expected b-tagging performance of the upgrade pixel detector at a luminosity of 2×10^{34} cm^{-2}s^{-1} is comparable to that for the current pixel detector with zero pileup (*i.e.* low luminosity) as shown in Fig. 10. Thus the upgrade pixel detector can almost entirely mitigate the expected degradation of b-tagging performance due to the efficiency loss and high occupancies caused by the pileup at the highest Phase 1 luminosities.

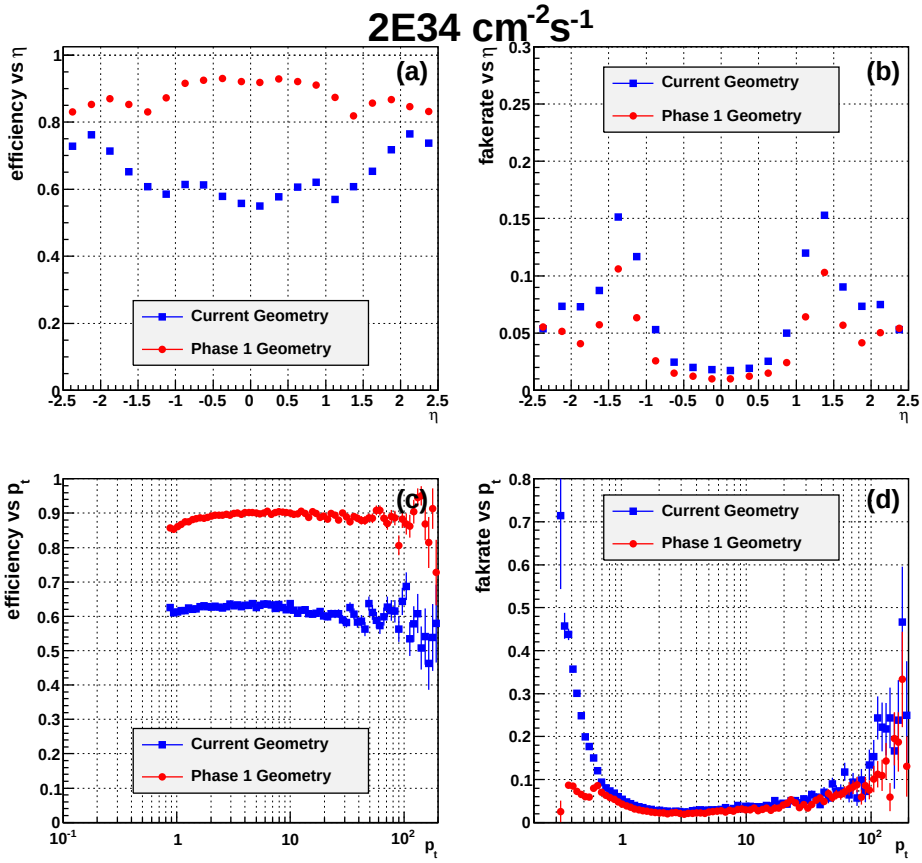

Fig. 9. Tracking efficiency and fake rates for $pp \rightarrow t\bar{t}X$ interactions at $\sqrt{s}$ = 14 TeV determined with a simulation study for a luminosity of 2×10^{34} cm^{-2}s^{-1} and assuming a crossing time of 25 ns. The results for the current pixel detector are shown in (blue) squares while those for the upgrade pixel detector are shown with (red) circles. Only statistical uncertainties are shown. Shown are tracking efficiencies for tracks from the $t\bar{t}$ (a) versus track η, and (b) versus track p_T. Track fake rates are shown (c) versus track η, and (d) versus track p_T.

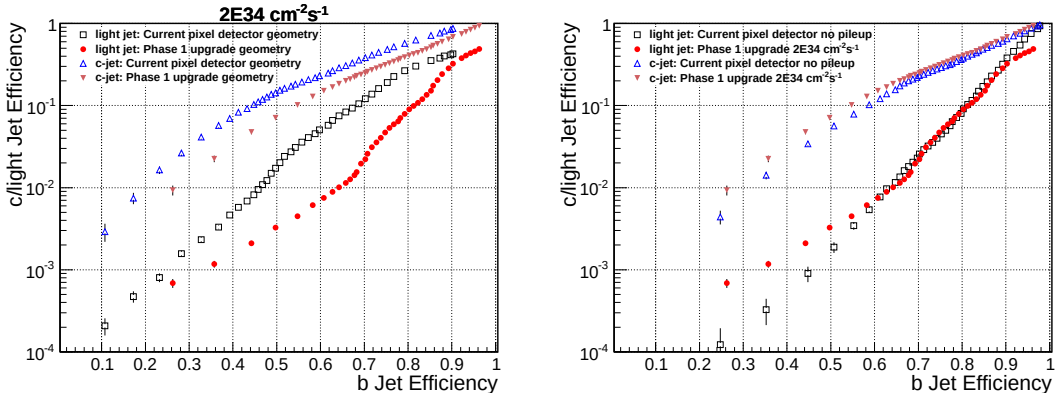

Fig. 10. Efficiency of tagging as a b-jet a real b-jet versus that for a c-jet or light quark (and gluon) jet using the combined secondary vertex b-tagging algorithm. Shown are the b-tagging performance with the current pixel detector (open points) and with the upgrade pixel detector (solid points). The triangular points are for c-jets versus b-jets, while the circular and square points are for light-quark and gluon jets versus b-jets. (Left) Comparing the b-tagging performance of the current and upgrade pixel detector at a luminosity of 2×10^{34} cm^{-2}s^{-1} and assuming a crossing time of 25 ns. (Right) Comparing the b-tagging performance of the upgrade pixel detector at a luminosity of 2×10^{34} cm^{-2}s^{-1} with that of the current pixel detector without pileup (low luminosity).

6. Other Subsystem Upgrades

Some of the upgrades to the subdetector systems necessitates upgrades to the Level 1 (L1) Trigger system. However the L1 output rate will be maintained at 100 KHz so the extra data (from additional channels in the upgraded detectors/readout) will be have to be handled by an upgraded data acquisition system (DAQ) [11]. One proposed upgrade to the L1 trigger is to implement in the regional calorimeter trigger the full granularity for internal processing, and more sophisticated clustering and isolation algorithms to handle the higher rates and more complex events. This upgrade is expected to give better position resolution and thus improve the trigger performance, *e.g.* in the isolated electron and isolated τ triggers [2]. A new infrastructure for the L1 trigger based on μTCA will be implemented to increase bandwidth and improve maintenance issues and provide the needed f exibility.

Details of the proposed upgrades to all the CMS subsystems and common CMS systems and infrastructure are given in the CMS proposal [2].

7. Phase 2 Upgrade R&D

For the Phase 2 period after 2020, the LHC is expected to deliver instantaneous luminosities of 5×10^{34} cm^{-2}s^{-1}. At these luminosities other upgrades of the CMS detector and trigger will be required to maintain the current level of performance for physics. For example, it is expected that the single muon L1 trigger rate can no longer be controlled simply by increasing the p_T threshold. Some tracking information is needed at L1 which will require a redesign and replacement of the entire CMS tracking system. The R&D for this as well as the other possible upgrades are currently being undertaken [2, 12].

8. Conclusions

Though the CMS detector has been working extremely well and expectations are great for making the most of the LHC luminosity, there have been a number of issues encountered so far. Some of these have been described and while none currently presents a problem for physics performance, some of them are expected to become more problematic, especially at the highest Phase 1 luminosities for which the majority of the integrated luminosity will be collected. These motivate upgrades for various parts of the CMS detector so that the current excellent physics performance can be maintained or even surpassed in the realm of the highest Phase 1 luminosities.

References

[1] S. Myers, "LHC Commissioning and First Operation" , ICHEP, Paris, France, 26 July 2010, `https://indico.cern.ch/contributionDisplay.py?contribId=73&confId=73513`.
[2] CMS Collaboration, "Technical Proposal for the Upgrade of the CMS Detector Through 2020", CERN-LHCC-2011-006, 2011/01/14, `http://cdsweb.cern.ch/record/1355706`.
[3] E. Focardi, "Status of the CMS Detector" , these proceedings.
[4] G. Bolla, "Status of the CMS pixel detector", International Workshop on Semiconductor Pixel Detectors for Particles and Imaging, Grindelwald, Switzerland, September 6–10, 2010.
[5] P. Karchin, "Performance of a Large-Area Triple-GEM Detector in a Particle Beam", these proceedings; T. Moulik, "Simulation of a Triple-GEM detector for a potential CMS muon tracking and trigger upgrade", these proceedings.
[6] CMS Collaboration, "Identif cation and f ltering of uncharacteristic noise in the CMS hadron calorimeter", 2010 JINST 5 T03014.
[7] J. Anderson, "Upgrade of the CMS Hadron Outer Calorimeter with SIPMs", these proceedings.
[8] S. Agostinelli *et al.*, "Geant4–a simulation toolkit", Nucl. Instrum. and Meth. in Phys. Research A 506 (2003) 250-303; and J. Allison *et al.*, "Geant4 developments and applications", IEEE Trans. on Nucl. Sc. 53 No. 1 (2006) 270-278.
[9] P. Jindal, "Tracking and b-tagging performance with an upgraded CMS pixel detector", these proceedings.
[10] C. Weiser, "A Combined Secondary Vertex Based B-Tagging Algorithm in CMS", CERN-CMS-NOTE-2006-014.
[11] F. Meijers, "Design, Operation and Future of the CMS DAQ system", these proceedings.
[12] S. Cihangir, "Silicon sensor R&D for an upgraded CMS Tracker in HL-LHC", these proceedings; L. Spiegel, "A tracker/trigger design for an upgraded CMS Tracker", these proceedings; G. Broccolo, "Design and studies of micro-strip stacked module prototypes for tracking at S-LHC", these proceedings; S. Mersi, "CMS Tracker layout studies for HL-LHC", these proceedings; P. Lamichhane, "Characterization of prototype silicon microstrip detectors for the CMS Tracker upgrade", these proceedings.